Article:

Tissue biomechanics during cranial neural tube closure measured by Brillouin microscopy and optical coherence tomography

Published: 2018

Journal: Wiley

Writers: Jitao Zhang Raksha Raghunathan Justin Rippy Chen Wu Richard H. Finnell Kirill V. Larin Giuliano Scarcelli

Department_bme

Received: 2 March 2018 | Revised: 3 July 2018 | Accepted: 2 August 2018

DOI: 10.1002/bdr2.1389

WILEY Birth Defects Research

RESEARCH ARTICLE

Tissue biomechanics during cranial neural tube closure measured by Brillouin microscopy and optical coherence tomography

Jitao Zhang[1] | Raksha Raghunathan[2] | Justin Rippy[2] | Chen Wu[2] | Richard H. Finnell[3] | Kirill V. Larin[2,3,4] | Giuliano Scarcelli[1]

[1]Fischell Department of Bioengineering, University of Maryland, Maryland

[2]Department of Biomedical Engineering, University of Houston, Houston, Texas

[3]Departments of Molecular and Cellular Biology and Medicine, Baylor College of Medicine, Houston, Texas

[4]Interdisciplinary Laboratory of Biophotonics, Tomsk State University, Tomsk, Russia

Correspondence
Kirill V. Larin, Department of Biomedical Engineering, University of Houston, Houston, Texas.
Email: klarin@uh.edu
and
Giuliano Scarcelli, Fischell Department of Bioengineering, University of Maryland, College Park, Maryland.
Email: scarc@umd.edu

Funding information
National Institutes of Health, Grant/Award Number: K25EB015885, R33CA204582, R01HD086765 R01HD081216, R01HD083809, P01HD067244, R01HL120140

Background: Embryonic development involves the interplay of driving forces that shape the tissue and the mechanical resistance that the tissue offers in response. While increasing evidence has suggested the crucial role of physical mechanisms underlying embryo development, tissue biomechanics is not well understood because of the lack of techniques that can quantify the stiffness of tissue *in situ* with 3D high-resolution and in a noncontact manner.

Methods: We used two all-optical techniques, optical coherence tomography (OCT) and Brillouin microscopy, to map the longitudinal modulus of the tissue from mouse embryos *in situ*.

Results: We acquired 2D mechanical maps of the neural tube region of embryos at embryonic day (E) 8.5 ($n = 2$) and E9.5 ($n = 2$) with submicron spatial resolution. We found the modulus of tissue varied distinctly within the neural tube region of the same embryo and between embryos at different development stages, suggesting our technique has enough sensitivity and spatial resolution to monitor the tissue mechanics during embryonic development in a noncontact and noninvasive manner.

Conclusions: We demonstrated the capability of OCT-guided Brillouin microscopy to quantify tissue longitudinal modulus of mouse embryos *in situ*, and observed distinct change in the modulus during the closure of cranial neural tube. Although this preliminary work cannot provide definitive conclusions on biomechanics of neural tube closure yet as a result of the limited number of samples, it provides an approach of quantifying the tissue mechanics during embryo development *in situ*, thus could be helpful in investigating the role of tissue biomechanics in the regulation of embryonic development. Our next study involving more embryo samples will investigate systematic changes in tissue mechanics during embryonic development.

KEYWORDS

Brillouin microscopy, development, embryo, OCT, tissue biomechanics

1 | INTRODUCTION

Extensive research efforts have uncovered how mechanical forces regulate cell functions through the process of mechanotransduction, a mechanism by which cells sense and convert mechanical stimuli to biochemical signals that elicit a range of specific cellular responses (Ingber, 2006; Vogel & Sheetz, 2006). Mechanical cues have also been found to play crucial roles during developmental processes (Barriga, Franze, Charras, & Mayor, 2018; Davidson, 2012; Davidson et al., 2010; Heer & Martin, 2017; Martin & Goldstein, 2014; Miller & Davidson, 2013; Schoenwolf & Smith, 1990; Wozniak & Chen, 2009), where the morphological evolution involving cell alignment, cell folding and tissue

Jitao Zhang and Raksha Raghunathan contributed equally to this study.

reshaping are contributed by both force and mechanical properties of local tissue. For example, the development of the central nervous system of vertebrate animals starts from neurulation, a folding process in which a flat neural plate is transformed into a closed neural tube, and the failure of this process may result in severe birth defect such as spina bifida (Blom, Shaw, den Heijer, & Finnell, 2006; Botto, Moore, Khoury, & Erickson, 1999; Copp & Greene, 2010; Copp, Stanier, & Greene, 2013; Wallingford, Niswander, Shaw, & Finnell, 2013). The process of neural tube closure (NTC) is regulated by biomechanics through the interaction of generated internal forces and the stiffness of the embryonic tissue (Nikolopoulou, Galea, Rolo, Greene, & Copp, 2017; Vijayraghavan & Davidson, 2017; Zhou, Pal, Maiti, & Davidson, 2015). Thus, understanding how the tissue deforms and reshapes under applied loads during NTC requires a detailed characterization of tissue biomechanics.

There exist many important techniques that highlight the crucial role of mechanics during embryonic development (Campas, 2016; Sugimura, Lenne, & Graner, 2016). Previously, the unconfined uniaxial compression test has been used to quantify the mechanical properties of the neural plate and dorsal tissue of the *Xenopus laevis* (African claw-toed frog), and it was determined that dorsal tissues had a stiffness that was more than four fold increased from gastrulation to neurulation (Zhou, Kim, & Davidson, 2009). However, the experiments were performed on isolated explants of dorsal tissue, and it would be challenging for *in situ* measurement as a result of the limitation of the method. Laser ablation uses an ultrashort pulsed laser to ablate a portion of a structure to create a mechanical imbalance that leads to a measureable response; thus, it can probe localized mechanics at both the cell and tissue scale in situ (Rauzi, Verant, Lecuit, & Lenne, 2008). Together with an imaging modality and a tissue-level strain-mapping workflow, Galea et al. (2017) have recently shown that the neural fold apposition of mouse embryo results from constriction of the open posterior neuropore, which is biomechanically coupled to the zippering point by an F-actin network. Laser ablation method is invasive, may introduce collateral damage, and its quantitative analysis requires the prior knowledge of either tension or material properties as they are always coupled together (Rauzi et al., 2008; Rauzi, Lenne, & Lecuit, 2010). Other indentation methods, such as cantilevers and atomic force microscopy (AFM), have been broadly used to quantify the stress–strain relation by applying force on the sample surface (Krieg et al., 2008). However, they all require physical contact and thus can only be performed on the surface of the tissue. Microrheology, optical tweezers, and magnetic tweezers measure the mechanical properties by monitoring the motion of beads injected into the cell or tissue (Daniels, Masi, & Wirtz, 2006; Weber, Bjerke, & DeSimone, 2012; Welte, Gross, Postner, Block, & Wieschaus, 1998). Several constraints have hindered their use in live embryonic tissue, including the risk of tissue damage upon injection of beads and the difficulty of calibration for quantitative measurement *in situ*. Elastography is a noninvasive method that maps the elastic properties of a sample from structural images of physical deformation induced by a known stress field (Kruse et al., 2000; Ophir et al., 2002; Schmitt, 1998). This is a promising technique, but its spatial resolution and precision are limited by the sensitivity and boundary conditions. Microdroplet-based sensor has successfully measured mechanical stresses by tracing the droplet's deformation after it is micro-injected between cells in tissue (Serwane et al., 2017), is limited to point-sample measurements. During embryonic development, the mechanical properties of the tissue experience both spatial and temporal regulation, which requires measuring techniques to have high spatial resolution within developing 3D tissues, and to be noninvasive and fast.

Spontaneous Brillouin light scattering is an optical phenomenon that arises from the interaction between incoming light and acoustic waves generated from fluctuation within the sample (Dil, 1982). Because of the Doppler effect, the scattered light undergoes an induced frequency shift (Brillouin shift) that is determined by the velocity of the acoustic wave. As the propagation of an acoustic wave is related to the mechanical properties of the material, Brillouin shift is directly linked to the longitudinal modulus (i.e., the ratio of uniaxial stress to uniaxial strain) of the material. As an all-optical technique, Brillouin spectroscopy based on Fabry–Perot interferometer (FPI) has long been used for material characterization (Vaughan & Randall, 1980) and remote environmental sensing (Hickman et al., 1991); however, FPI-based Brillouin spectroscopy requires long acquisition times. In 2008, a parallel dispersive imaging spectrometer based on a virtually imaged phased array (VIPA) was first developed and combined with a confocal microscope to enable Brillouin imaging (Scarcelli & Yun, 2008).

Brillouin microscopy has been recently used to characterize the mechanical properties of eye tissue (Besner, Scarcelli, Pineda, & Yun, 2016; Scarcelli, Besner, Pineda, Kalout, & Yun, 2015) in vivo, fibrous proteins of the extracellular matrix (Palombo et al., 2014), and cellular mechanics (Antonacci & Braakman, 2016; Elsayad et al., 2016; Scarcelli et al., 2015; Zhang, Nou, Kim, & Scarcelli, 2017). Very recently, we acquired the first mechanical images of a mouse embryo with the Brillouin microscope (Raghunathan et al., 2017), demonstrating that this technique had the promising capability of characterizing the biomechanics of embryonic tissue *in situ*.

Optical coherence tomography (OCT) (Huang et al., 1991) is a well-developed optical imaging modality capable of live 4D embryonic imaging with high spatial and temporal resolutions (Wang et al., 2015). Because of its ability to provide high-resolution cross-sectional images, OCT has been preferred over other imaging modalities for small animal embryos (Raghunathan, Singh, Dickinson, & Larin,

2016). Although histological sectioning has been the gold standard for embryonic imaging, its invasive and time consuming nature combined with the necessity to fix the tissue makes live imaging impossible (Walls, Coultas, Rossant, & Henkelman, 2008). Other noninvasive imaging modalities such as ultrasound biomicroscopy (UBM), micro-magnetic resonance imaging (micro-MRI), and micro-computed tomography (micro-CT) have been used to image small animal embryos. However, limited spatial resolution of UBM (Foster, Zhang, Duckett, Cucevic, & Pavlin, 2003; Phoon & Turnbull, 2003), long acquisition times of micro-MRI and its use of external contrast agents (Nieman et al., 2005), and ionizing radiation in micro-CT are all undesirable for imaging live embryos (Badea, 2018).

Here, with the help of the structural guidance provided by OCT, we demonstrated the mechanical mapping of the neural tube at the cranial region during the early development of mouse embryo by using a Brillouin microscope. Within this preliminary study, we found that the dorsal tissue was distinctly stiffened over time as the embryos developed from embryonic day (E) 8.5 ($n = 2$) to E9.5 ($n = 2$). Specifically, after NTC (E9.5), we found that the tissue at the point of fusion was softer than that in the adjacent region, and the modulus of the dorsal tissue itself had a gradient along dorsal–ventral direction. In addition, we identified the ectodermal layer that covered the closed neural tube based on Brillouin metric, and found it was generally softer than the dorsal tissue. This work indicates that tissue mechanics probably changes significantly during the closure of cranial neural tube, and it is thus worthy to further investigate if tissue mechanics plays crucial role during normal development of embryo.

2 | MATERIALS AND METHODS

2.1 | Embryo preparation

CD-1 mice were set up for timed overnight mating and were checked for a vaginal plug every morning. The presence of a vaginal plug was considered E 0.5. On E8.5 (n = 2) and E9.5 (n = 2), the mother was euthanized by carbon dioxide inhalation and the embryos were dissected out. These embryos were then embedded in 1% agarose with phosphate-buffered saline before being imaged using a home-built swept source OCT system at the University of Houston. All procedures were performed under an approved protocol by the University of Houston Institutional Animal Care and Use Committee. The embryos embedded in agar were first imaged with OCT at the University of Houston and immediately transported to the University of Maryland on ice and imaged with Brillouin microscopy, within 24 hr. The embryos were embedded in agarose to maintain the same orientation of the embryo while being imaged using both modalities. This helped us to image the same region of the neural tube despite having to transport embryos between campuses.

2.2 | OCT setup

The OCT system consisted of a swept source laser (HSL2000, Santec USA, Corp., Hackensack, NJ) with a central wavelength of ~1,310 nm, scan range of ~150 nm, A-scan rate of ~30 kHz, output power of ~39 mW, and axial resolution of ~11 μm (in air). More information on the system can be found in our previous work (Manapuram, Manne, & Larin, 2008). The images were rescaled to physical dimensions by assuming that the refractive indices of 1% agarose and the embryos were 1.38.

2.3 | Brillouin microscopy

The configuration of the Brillouin microscope has been previously reported (Raghunathan et al., 2017; Scarcelli, Polacheck, et al., 2015). Briefly, a two-stage VIPA spectrometer was used to acquire the Brillouin signal (Scarcelli, Kim, & Yun, 2011), and a spectral coronagraphy was integrated into the spectrometer to enhance its noise-rejection capability (Edrei, Gather, & Scarcelli, 2017). An objective lens with an effective numerical aperture of 0.4 was used to achieve a spatial resolution of 0.8 μm × 0.8 μm × 3.3 μm. The acquisition time of the spectrometer was 50 ms for single point measurement. The 2D Brillouin imaging was acquired by scanning the embryo with a 3D motorized stage. The scanning step size was set as 4 and 1 μm in lateral and axial direction, respectively. During measurement, the cross sections around the cranial region of the embryo were mapped by Brillouin microscope, which was guided by the 3D image previously acquired with OCT (Figure 1).

The measured Brillouin shift ν_B of the backward scattered light is related to the longitudinal modulus M' of the sample via the relationship $\nu_B = 2n/\lambda \cdot \sqrt{M'/\rho}$, where n is the refractive index, λ is the laser wavelength, and ρ is the material density. Previous experiments indicate that M' has a linear relationship with Young's modulus E' under log–log scale (Scarcelli et al., 2011); thus the relative changes of longitudinal modulus and Young's modulus can be approximated as $\delta E'/E' = (1/a)\delta M'/M'$, where a is a factor related to the material. For cells, $1/a$ has been calibrated to be ~15 (Scarcelli, Polacheck, et al., 2015). For ruminant retina tissue, this relationship was still valid and $1/a$ was estimated to be ~14.3 (Weber, Yun, Scarcelli, & Franze, 2017). We used these values to estimate the elastic modulus change of neural tube tissue of embryos.

3 | RESULTS

3.1 | Tissue stiffens significantly after NTC

Previous measurements on *X. laevis* embryos reported tissue stiffening during the stage of elongation and NTC (Barriga et al., 2018; Zhou et al., 2009). In our studies using a mouse model, we initially observed tissue stiffening of the neural

FIGURE 1 Representative 3D images of mouse embryos acquired by OCT. (a) E8.5 and (b) E9.5. The red dashed line indicated the cross section of the neural tube scanned by Brillouin microscope. Both scale bars are 100 μm

folds by comparing embryos with open (E8.5) and closed (E9.5) neural tubes (Figure 2). The representative morphologies of two embryos was imaged with OCT (Figure 2a,b), where the open and closed neural tube can be clearly seen. As shown in the colocalized Brillouin images, the closed neural tube (Figure 2d) is distinctly stiffer than the opened neural tube (Figure 2c). We quantified the averaged Brillouin shift of the whole neural tube region (Figure 2e), and the results suggest that the Brillouin shift of the closed neural tube is 0.21 GHz higher than an opened one. Using a previous calibration between Brillouin-derived longitudinal modulus and Young's modulus (Section 2), this amount of frequency change would correspond to ~80% relative increase of Young's modulus ($\delta E'/E'$).

3.2 | Modulus of neural tube tissue has a gradient along dorsal–ventral direction and fusion region is much softer after closure

We next assessed the modulus distribution on the neural folds after NTC. For this analysis, we scanned cross-sections at different locations close to the cranial neuropore of a E9.5 embryo (Figure 3). The OCT images suggest that the neural tubes are fully closed in all three locations (Figure 3a–3c), while the colocalized Brillouin images indicate there exists a modulus gradient along the neural tube (Figure 3d–3f). To quantify this variation, we first divided an individual neural tube into multiple subregions according to the modulus distribution, as indicated by the red box. We next calculated the average Brillouin shift in each subregion, and the results are shown in Figure 3g–3i. We first noticed that the Brillouin shift of the fusion region is much smaller than that of the adjacent neural folds. The differences of Brillouin shift are within a range between 0.14 and 0.28 GHz, indicating the adjacent neural tube is 60%–100% stiffer than the fusion region in terms of Young's modulus. The curves in Figure 3g–3i also suggest a modulus decrease in the neural tube from dorsal region to ventral region (green arrows). As we did not observe similar phenomena in the open neural tube of E8.5 embryo, we hypothesize that this modulus gradient is related to the translocation of neuroepithelial cells in ventral–dorsal direction during later development (McShane et al., 2015), and may play crucial role in facilitating the successful closure of the neural tube.

3.3 | Ectoderm layer can be distinguished from neural tube and is much softer

The closed neural tube is covered by a surface ectoderm which is usually indistinguishable from adjacent dorsal tissue without utilizing some variety of cell labeling (Figure 3a,c). Using a mechanical phenotype as a signature, we can clearly distinguish the ectoderm layer from the neural tube tissue, as outlined by the dashed white line in Figure 4a–4c). We subsequently quantified the modulus difference between the ectodermal layer and the neural tube tissue. For this purpose, we excluded the fusion region and outlined the neural tube as left side and right side; we then calculated the average Brillouin shift of each region (Figure 4d–4f). We found that although the Brillouin shift of the left and right sides of the neural tube are quite close, the ectoderm layer has a much smaller Brillouin shift (0.22 GHz). This suggests that the ectoderm layer is approximately 80.4% softer than the closed neural tube in terms of the Young's modulus.

4 | DISCUSSION

The process of neural tube fusion and closure involves several critically important cell activities such as apical constriction, convergent extension, and cell migration, which facilitate NTC by thickening, lengthening, elevating and bending the neural tube tissue. The tissue stiffening we observed with Brillouin technique could be a consequence of such cell activities. For example, a previous study has observed an increase in cell density dorsolaterally compared with the more ventromedial neural folds, which is caused by both the translocation of neuroepithelial cells in a ventral-to-dorsal direction, and rapid cell proliferation locally (McShane et al., 2015). As the tissue stiffness is closely related to the cell density (Koser, Moeendarbary, Hanne, Kuerten, & Franze, 2015; Weber et al., 2017), the modulus gradient we observed in Figure 3 could be also related to cell translocations, which will need to be investigated and verified in future studies. The tissue stiffening also suggests that the force generated by actomyosin may also need to be increased accordingly to accomplish a successful closure.

In the late stage of NTC, the cellular protrusions from the leading edge of the apposed neural folds make initial contacts between the folds and achieve the epithelial adhesion (Pai et al., 2012), which eventually results in a stable epithelial fusion across the midline of the neural tube. The distinctly soft region at the midline shown in Figure 3

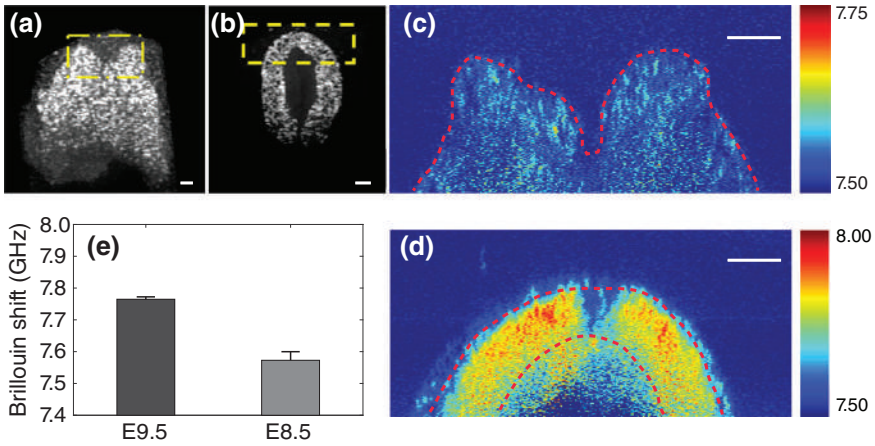

FIGURE 2 Tissue stiffening of the neural tube during embryonic development. OCT cross-sectional images of representative (a) E8.5 and (b) E9.5 embryos. Dashed yellow boxes indicate the imaged region by Brillouin microscope. (c and d) corresponding Brillouin images at the same cross sections; the red dashed lines indicate the neural folds. (e) Averaged Brillouin shift of the neural tube tissues of E8.5 ($n = 2$) and E9.5 ($n = 2$) embryos. All scale bars are 100 μm

provides a hint of epithelial fusion during NTC and suggests that it has a different mechanical phenotype from that of the neural folds.

It is important to note that the mechanical property sensed by Brillouin technique is a high-frequency longitudinal modulus M', whose relation to quasi-static Young's modulus E' measured by conventional method is not clearly known. However, several empirical studies have found the two types of moduli to be correlated (Scarcelli et al., 2011; Scarcelli, Polacheck, et al., 2015; Weber et al., 2017). For an accurate conversion from M' to E', a material-dependent calibration is required; here, we have estimated the relative changes of Young's modulus of neural tube tissue based on a previous calibration based on retina tissue. In future, a direct calibration on neural tube tissue will be necessary.

Besides the longitudinal modulus, the value of Brillouin shift is also related to the density and refractive index of the tissue, the effects of which have not been evaluated with the current technique. However, previous studies suggest that these two parameters are usually coupled with each other for biological samples such as cells and tissues (Barer, Ross, & Tkaczyk, 1953; Schürmann, Scholze, Müller, Guck, & Chan, 2016), and the ratio of $n/\sqrt{\rho}$ is nearly constant for cells (Scarcelli, Polacheck, et al., 2015). In the future, a

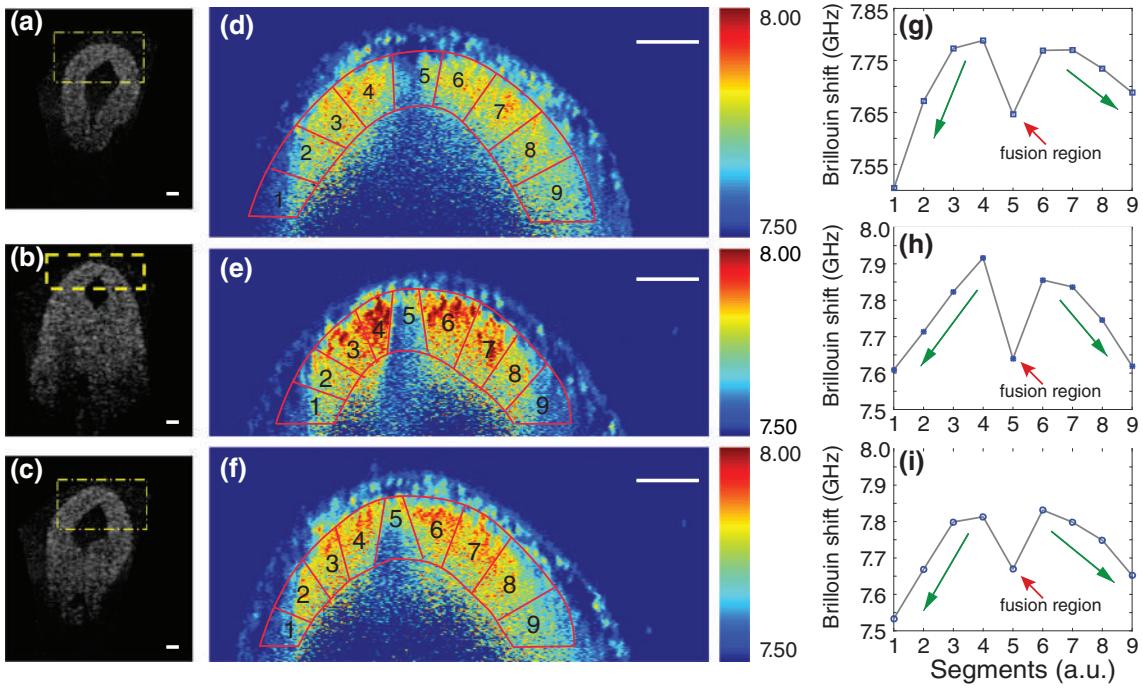

FIGURE 3 Tissue modulus of the neural folds shows a gradient along dorsal–ventral direction. (a–c) OCT cross-sectional images of the neural tube of a representative E9.5 mouse embryo. Dashed yellow boxes indicate the imaged region by Brillouin microscopy. (d–f) Corresponding Brillouin images at the same cross sections; the neural tube is artificially segmented into different subregions (red lines) to quantify averaged modulus locally, and the results are shown in panels g–i. Red arrows indicate the region of neural tube fusion is distinctly softer than other part of neural folds; green arrows indicate the curve trend. All scale bars are 100 μm

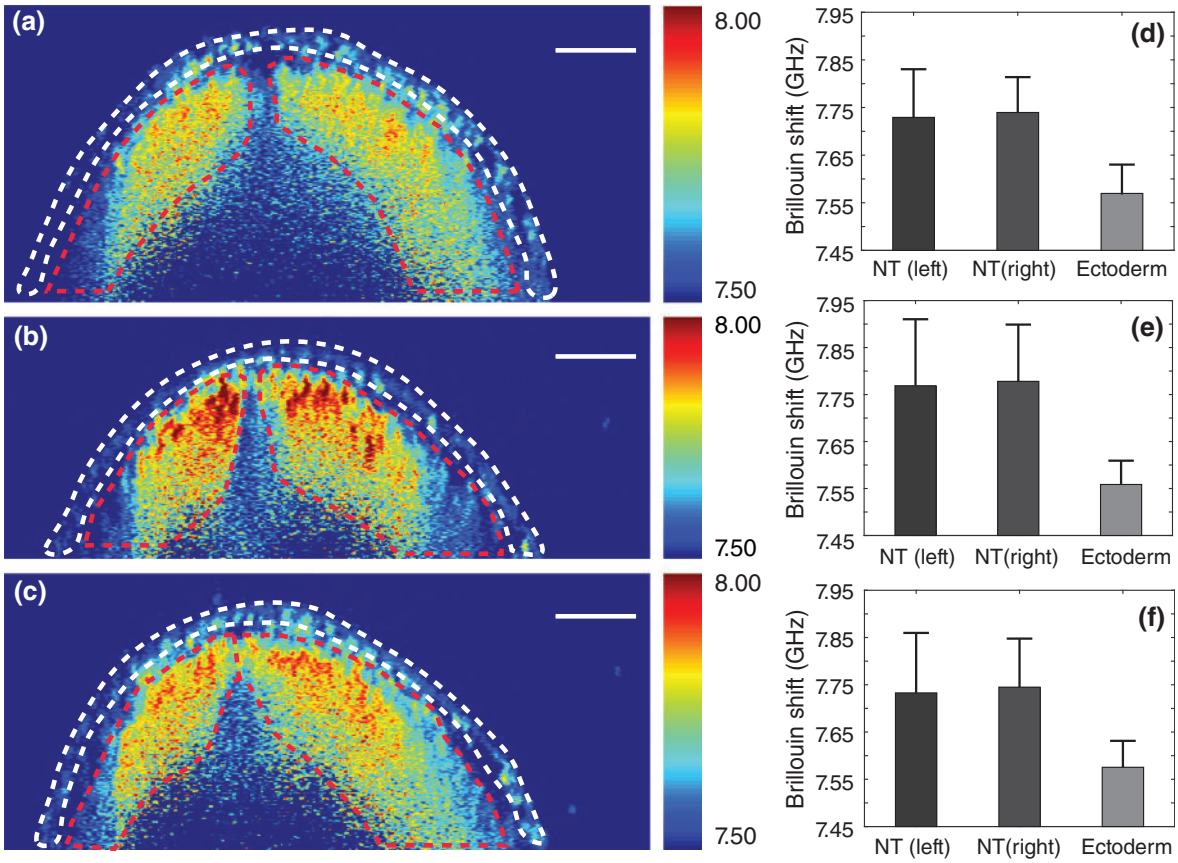

FIGURE 4 (a–c) Brillouin images of neural tubes at different levels of a representative E9.5 embryo (same as Figure 3d,f); (d–f) averaged Brillouin shifts (mean ±S.D.) of neural tube tissues (region indicated by red dashed line) and ectoderm layers (region indicated by white dashed line); NT (left) and NT (right) indicate the left and right part of the neural fold, respectively. All scale bars are 100 μm

direct measurement of refractive index and/or density of embryonic tissue would be necessary for accurate determination of the longitudinal modulus. Additionally, as these measurements were conducted post-mortem, the absolute values of M' (and E') might be somewhat different in live embryos; however, the contrast expected to be the same—subject of our future studies.

Because of the elastic scattering from embryonic tissue, the Brillouin signal dropped quickly as the image depth increased. The penetration depth of our current Brillouin setup is therefore limited to ~200 μm. This limitation could be mitigated by using an advanced illumination strategy based on adaptive optics technique (Edrei & Scarcelli, 2018).

The sample numbers in this study was limited because of issues encountered during transportation of samples between the two labs. This does not allow us to draw general conclusions on biomechanics of NTC yet. A following study that involves larger number of embryo samples will be conducted to systematically investigate qualitative changes in tissue mechanics during the closure of neural tube.

5 | CONCLUSION

Embryogenesis is an intrinsically biomechanical process that involves the interplay of driving forces that shape the tissue morphology and the mechanical resistance that the tissue offers as a response. The mechanical properties of the embryonic tissue thus are crucial during the development. Although increasing attention has been paid to understanding the importance of mechanical cues during development, the mechanical properties of embryonic tissue are not fully characterized because of a lack of availability of a proper technique. Within this preliminary work, by using OCT and Brillouin microscopy, we observed the biomechanical changes in murine embryonic tissue during early development. We demonstrated that this novel technology was sensitive to the mechanical change of the neural tube tissue during the course of NTC, indicating the promising capability of the Brillouin technique in quantifying tissue biomechanics during embryogenesis.

ACKNOWLEDGMENTS

This work is supported by National Institute of Health under contract numbers: R01HD081216, R01HD083809, P01HD0 67244, R01HL120140, K25 EB015885, R33CA204582, and R01HD086765.

CONFLICT OF INTERESTS

The authors report no declaration of interest.

ORCID

Jitao Zhang http://orcid.org/0000-0002-6240-0371

REFERENCES

Antonacci, G., & Braakman, S. (2016). Biomechanics of subcellular structures by non-invasive Brillouin microscopy. *Scientific Reports*, *6*, 37217.

Badea, C. T. (2018). Small animal X-ray computed tomography. In *Handbook of X-ray imaging: Physics and technology*. Boca Raton: CRC Press.

Barer, R., Ross, K., & Tkaczyk, S. (1953). Refractometry of living cells. *Nature*, *171*(4356), 720–724.

Barriga, E. H., Franze, K., Charras, G., & Mayor, R. (2018). Tissue stiffening coordinates morphogenesis by triggering collective cell migration in vivo. *Nature*, *554*, 523–527.

Besner, S., Scarcelli, G., Pineda, R., & Yun, S.-H. (2016). In vivo Brillouin analysis of the aging crystalline lens. *Investigative Ophthalmology & Visual Science*, *57*(13), 5093–5100.

Blom, H. J., Shaw, G. M., den Heijer, M., & Finnell, R. H. (2006). Neural tube defects and folate: Case far from closed. *Nature Reviews Neuroscience*, *7*(9), 724–731.

Botto, L. D., Moore, C. A., Khoury, M. J., & Erickson, J. D. (1999). Neural-tube defects. *The New England Journal of Medicine*, *341*(20), 1509–1519.

Campas, O. (2016). A toolbox to explore the mechanics of living embryonic tissues. *Seminars in Cell & Developmental Biology*, *55*, 119–130.

Copp, A. J., & Greene, N. D. (2010). Genetics and development of neural tube defects. *The Journal of Pathology*, *220*(2), 217–230.

Copp, A. J., Stanier, P., & Greene, N. D. (2013). Neural tube defects: Recent advances, unsolved questions, and controversies. *The Lancet Neurology*, *12*(8), 799–810.

Daniels, B. R., Masi, B. C., & Wirtz, D. (2006). Probing single-cell micromechanics in vivo: The microrheology of C. Elegans developing embryos. *Biophysical Journal*, *90*(12), 4712–4719.

Davidson, L. A. (2012). Epithelial machines that shape the embryo. *Trends in Cell Biology*, *22*(2), 82–87.

Davidson, L. A., Joshi, S. D., Kim, H. Y., Von Dassow, M., Zhang, L., & Zhou, J. (2010). Emergent morphogenesis: Elastic mechanics of a self-deforming tissue. *Journal of Biomechanics*, *43*(1), 63–70.

Dil, J. (1982). Brillouin scattering in condensed matter. *Reports on Progress in Physics*, *45*(3), 285–334.

Edrei, E., Gather, M. C., & Scarcelli, G. (2017). Integration of spectral coronagraphy within VIPA-based spectrometers for high extinction Brillouin imaging. *Optics Express*, *25*(6), 6895–6903.

Edrei, E., & Scarcelli, G. (2018). Brillouin micro-spectroscopy through aberrations via sensorless adaptive optics. *Applied Physics Letters*, *112*(16), 163701.

Elsayad, K., Werner, S., Gallemi, M., Kong, J., Sanchez Guajardo, E. R., Zhang, L., … Belkhadir, Y. (2016). Mapping the subcellular mechanical properties of live cells in tissues with fluorescence emission-Brillouin imaging. *Science Signaling*, *9*(435), rs5.

Foster, F. S., Zhang, M., Duckett, A. S., Cucevic, V., & Pavlin, C. J. (2003). In vivo imaging of embryonic development in the mouse eye by ultrasound biomicroscopy. *Investigative Ophthalmology & Visual Science*, *44*(6), 2361–2366.

Galea, G. L., Cho, Y. J., Galea, G., Mole, M. A., Rolo, A., Savery, D., … Copp, A. J. (2017). Biomechanical coupling facilitates spinal neural tube closure in mouse embryos. *Proceedings of the National Academy of Sciences of the United States of America*, *114*(26), E5177–e5186.

Heer, N. C., & Martin, A. C. (2017). Tension, contraction and tissue morphogenesis. *Development*, *144*(23), 4249–4260.

Hickman, G. D., Harding, J. M., Carnes, M., Pressman, A., Kattawar, G. W., & Fry, E. S. (1991). Aircraft laser sensing of sound velocity in water: Brillouin scattering. *Remote Sensing of Environment*, *36*(3), 165–178.

Huang, D., Swanson, E. A., Lin, C. P., Schuman, J. S., Stinson, W. G., Chang, W., … Puliafito, C. A. (1991). Optical coherence tomography. *Science*, *254*(5035), 1178–1181.

Ingber, D. E. (2006). Cellular mechanotransduction: Putting all the pieces together again. *The FASEB Journal*, *20*(7), 811–827.

Koser, D., Moeendarbary E., Hanne J., Kuerten S., & Franze K. (2015). CNS cell distribution and axon orientation determine local spinal cord mechanical properties. *Biophys J*, *108*(9), 2137–2147.

Krieg, M., Arboleda-Estudillo, Y., Puech, P. H., Käfer, J., Graner, F., Müller, D. J., & Heisenberg, C. P. (2008). Tensile forces govern germ-layer organization in zebrafish. *Nature Cell Biology*, *10*, 429–436.

Kruse, S. A., Smith, J. A., Lawrence, A. J., Dresner, M. A., Manduca, A., Greenleaf, J. F., & Ehman, R. L. (2000). Tissue characterization using magnetic resonance elastography: Preliminary results. *Physics in Medicine and Biology*, *45*(6), 1579–1590.

Manapuram, R., Manne, V., & Larin, K. (2008). Development of phase-stabilized swept-source OCT for the ultrasensitive quantification of microbubbles. *Laser Physics*, *18*(9), 1080–1086.

Martin, A. C., & Goldstein, B. (2014). Apical constriction: Themes and variations on a cellular mechanism driving morphogenesis. *Development*, *141*(10), 1987–1998.

McShane, S. G., Mole, M. A., Savery, D., Greene, N. D., Tam, P. P., & Copp, A. J. (2015). Cellular basis of neuroepithelial bending during mouse spinal neural tube closure. *Developmental Biology*, *404*(2), 113–124.

Miller, C. J., & Davidson, L. A. (2013). The interplay between cell signalling and mechanics in developmental processes. *Nature Reviews Genetics*, *14*(10), 733–744.

Nieman, B. J., Bock, N. A., Bishop, J., Chen, X. J., Sled, J. G., Rossant, J., & Henkelman, R. M. (2005). Magnetic resonance imaging for detection and analysis of mouse phenotypes. *NMR in Biomedicine*, *18*(7), 447–468.

Nikolopoulou, E., Galea, G. L., Rolo, A., Greene, N. D., & Copp, A. J. (2017). Neural tube closure: Cellular, molecular and biomechanical mechanisms. *Development*, *144*(4), 552–566.

Ophir, J., Alam, S. K., Garra, B. S., Kallel, F., Konofagou, E. E., Krouskop, T., … Varghese, T. (2002). Elastography: Imaging the elastic properties of soft tissues with ultrasound. *Journal of Medical Ultrasonics*, *29*(4), 155–171.

Pai, Y. J., Abdullah, N. L., Mohd-Zin, S. W., Mohammed, R. S., Rolo, A., Greene, N. D., … Copp, A. J. (2012). Epithelial fusion during neural tube morphogenesis. *Birth Defects Research. Part A, Clinical and Molecular Teratology*, *94*(10), 817–823.

Palombo, F., Winlove, C. P., Edginton, R. S., Green, E., Stone, N., Caponi, S., … Fioretto, D. (2014). Biomechanics of fibrous proteins of the extracellular matrix studied by Brillouin scattering. *Journal of the Royal Society Interface*, *11*(101), 20140739.

Phoon, C. K., & Turnbull, D. H. (2003). Ultrasound biomicroscopy-Doppler in mouse cardiovascular development. *Physiological Genomics*, *14*(1), 3–15.

Raghunathan R, Singh M, Dickinson ME, Larin KV. 2016. Optical coherence tomography for embryonic imaging: A review. *Journal of Biomedical Optics* *21*(5):50902, 050902.

Raghunathan, R., Zhang, J., Wu, C., Rippy, J., Singh, M., Larin, K. V., & Scarcelli, G. (2017). Evaluating biomechanical properties of murine embryos using Brillouin microscopy and optical coherence tomography. *Journal of Biomedical Optics*, *22*(8), 086013.

Rauzi, M., Lenne, P. F., & Lecuit, T. (2010). Planar polarized actomyosin contractile flows control epithelial junction remodelling. *Nature*, *468*(7327), 1110–1114.

Rauzi, M., Verant, P., Lecuit, T., & Lenne, P.-F. (2008). Nature and anisotropy of cortical forces orienting drosophila tissue morphogenesis. *Nature Cell Biology*, *10*, 1401–1410.

Scarcelli, G., Besner, S., Pineda, R., Kalout, P., & Yun, S. H. (2015). In vivo biomechanical mapping of normal and keratoconus corneas. *JAMA Ophthalmology*, *133*(4), 480–482.

Scarcelli, G., Kim, P., & Yun, S. H. (2011). In vivo measurement of age-related stiffening in the crystalline lens by Brillouin optical microscopy. *Biophysical Journal*, *101*(6), 1539–1545.

Scarcelli, G., Polacheck, W. J., Nia, H. T., Patel, K., Grodzinsky, A. J., Kamm, R. D., & Yun, S. H. (2015). Noncontact three-dimensional mapping of intracellular hydromechanical properties by Brillouin microscopy. *Nature Methods*, *12*(12), 1132–1134.

Scarcelli, G., & Yun, S. H. (2008). Confocal Brillouin microscopy for three-dimensional mechanical imaging. *Nature Photonics*, *2*(1), 39–43.

Schmitt, J. (1998). OCT elastography: Imaging microscopic deformation and strain of tissue. *Optics Express*, *3*(6), 199–211.

Schoenwolf, G. C., & Smith, J. L. (1990). Mechanisms of neurulation: Traditional viewpoint and recent advances. *Development*, *109*(2), 243–270.

Schürmann, M., Scholze, J., Müller, P., Guck, J., & Chan, C. J. (2016). Cell nuclei have lower refractive index and mass density than cytoplasm. *Journal of Biophotonics*, *9*(10), 1068–1076.

Serwane, F., Mongera, A., Rowghanian, P., Kealhofer, D. A., Lucio, A. A., Hockenbery, Z. M., & Campas, O. (2017). In vivo quantification of spatially varying mechanical properties in developing tissues. *Nature Methods*, *14*(2), 181–186.

Sugimura, K., Lenne, P.-F., & Graner, F. (2016). Measuring forces and stresses in situ in living tissues. *Development*, *143*(2), 186–196.

Vaughan, J. M., & Randall, J. T. (1980). Brillouin scattering, density and elastic properties of the lens and cornea of the eye. *Nature*, *284*, 489–491.

Vijayraghavan, D. S., & Davidson, L. A. (2017). Mechanics of neurulation: From classical to current perspectives on the physical mechanics that shape, fold, and form the neural tube. *Birth Defects Research*, *109*(2), 153–168.

Vogel, V., & Sheetz, M. (2006). Local force and geometry sensing regulate cell functions. *Nature Reviews. Molecular Cell Biology*, *7*(4), 265–275.

Wallingford, J. B., Niswander, L. A., Shaw, G. M., & Finnell, R. H. (2013). The continuing challenge of understanding, preventing, and treating neural tube defects. *Science*, *339*(6123), 1222002.

Walls, J. R., Coultas, L., Rossant, J., & Henkelman, R. M. (2008). Three-dimensional analysis of vascular development in the mouse embryo. *PLoS One*, *3*(8), e2853.

Wang, S., Singh, M., Lopez, A. L., 3rd, Wu, C., Raghunathan, R., Schill, A., … Larina, I. V. (2015). Direct four-dimensional structural and functional imaging of cardiovascular dynamics in mouse embryos with 1.5 MHz optical coherence tomography. *Optics Letters*, *40*(20), 4791–4794.

Weber, G. F., Bjerke, M. A., & DeSimone, D. W. (2012). A mechanoresponsive cadherin-keratin complex directs polarized protrusive behavior and collective cell migration. *Developmental Cell*, *22*(1), 104–115.

Weber, I. P., Yun, S. H., Scarcelli, G., & Franze, K. (2017). The role of cell body density in ruminant retina mechanics assessed by atomic force and Brillouin microscopy. *Physical Biology*, *14*(6), 065006.

Welte, M. A., Gross, S. P., Postner, M., Block, S. M., & Wieschaus, E. F. (1998). Developmental regulation of vesicle transport in drosophila embryos: Forces and kinetics. *Cell*, *92*(4), 547–557.

Wozniak, M. A., & Chen, C. S. (2009). Mechanotransduction in development: A growing role for contractility. *Nature Reviews. Molecular Cell Biology*, *10*(1), 34–43.

Zhang, J., Nou, X. A., Kim, H., & Scarcelli, G. (2017). Brillouin flow cytometry for label-free mechanical phenotyping of the nucleus. *Lab on a Chip*, *17*(4), 663–670.

Zhou, J., Kim, H. Y., & Davidson, L. A. (2009). Actomyosin stiffens the vertebrate embryo during crucial stages of elongation and neural tube closure. *Development*, *136*(4), 677–688.

Zhou, J., Pal, S., Maiti, S., & Davidson, L. A. (2015). Force production and mechanical accommodation during convergent extension. *Development*, *142*(4), 692–701.

How to cite this article: Zhang J, Raghunathan R, Rippy J, et al. Tissue biomechanics during cranial neural tube closure measured by Brillouin microscopy and optical coherence tomography. *Birth Defects Research*. 2018;1–8. https://doi.org/10.1002/bdr2.1389

Contact us

@department_bme

@department_bme

@department_bme

Info@dep-bme.ir

www.dep-bme.ir

Department of Biomedical engineering